

A DISCRETE-ORDINATE DISCONTINUOUS-STREAMLINE DIFFUSION METHOD FOR THE RADIATIVE TRANSFER EQUATION

CHENG WANG[†], QIWEI SHENG[‡], AND WEIMIN HAN[§]

ABSTRACT. The radiative transfer equation (RTE) arises in many different areas of science and engineering. In this paper, we propose and investigate a discrete-ordinate discontinuous-streamline diffusion (DODSD) method for solving the RTE, which is a combination of the discrete-ordinate technique and the discontinuous-streamline diffusion method. Different from the discrete-ordinate discontinuous Galerkin (DODG) method for the RTE, an artificial diffusion parameter is added to the test functions in the spatial discretization. Stability and error estimates in certain norms are proved. Numerical results show that the proposed method can lead to a more accurate approximation in comparison with the DODG method.

Key words. radiative transfer equation, discrete-ordinate method, discontinuous-streamline diffusion method, stability, error estimation

AMS subject classifications. 65N30, 65R20

1. INTRODUCTION

The radiative transfer equation, which describes the scattering and absorbing of radiation through a medium, plays an important role in a wide range of applications such as astrophysics, atmosphere and ocean, heat transfer, neutron transport and nuclear physics, and so on. Today, research on the RTE remains to be very active and important, especially in the biomedical optics fields, see e.g. [2, 6, 14, 26, 28].

The RTE can be viewed as a hyperbolic type integro-differential equation. Due to the involvement of both integration and differentiation in the equation, as well as the high dimension of the problem, it is challenging to develop effective numerical methods for solving the RTE. The numerical methods can be basically divided into two categories: statistical schemes and deterministic schemes. The interested readers are referred to [11, 12, 13, 15, 17, 19, 24, 25, 27].

The discrete-ordinate (DO) method [8, 22, 23], also called the S_N method, is the most popular deterministic method for the RTE, owing to the good compromise among accuracy, flexibility, and moderate computational requirements. This method solves the radiative transfer equation along a discrete set of angular directions, which are the nodal points of a numerical quadrature approximating the integral term on the unit sphere, thus reducing the RTE to a semi-discretized first-order hyperbolic system. To solve the semi-discretized

[†] Department of Mathematics, Tongji University, Shanghai 200092, China (wangcheng@tongji.edu.cn).

[‡] Computational and Applied Mathematics Group, Oak Ridge National Laboratory, Oak Ridge, TN 37831 (shengqi@ornl.gov).

[§] Department of Mathematics, University of Iowa, Iowa City, IA 52242 (weimin-han@uiowa.edu).

hyperbolic system, it is natural to use the discontinuous Galerkin (DG) discretization, leading to the so-called discrete-ordinate discontinuous Galerkin method. In [16], a DODG method was proposed for the RTE, and error estimates in certain discrete norms were obtained.

The object of this paper is to propose and investigate a discrete-ordinate discontinuous-streamline diffusion method for solving the RTE. Such a method is a combination of the discrete-ordinate technique and the discontinuous-streamline diffusion (DSD) method. The streamline diffusion (SD) finite element method was proposed by Hughes et al. [20] and Johnson et al. [21] in order to cope with the usual instabilities caused by the convection term for the convection-dominated problem. In [3, 4], the streamline diffusion finite element method was analyzed for the multi-dimensional Vlasov-FokkerPlanck system and Fermi pencil beam equation. The DSD method keeps the fundamental structure of the DG method while replacing the Galerkin elements by the SD framework in the upwind iteration procedure. In [9], the DSD method was employed successfully in solving first order hyperbolic problems, where such a modification preserves the advantages of both the upwind approach and the DG method, and also further improves the stability. In this contribution, we seek to improve the DG method for RTE by employing the DSD scheme and derive error estimates of the DODSD method in a norm including the directional gradient. While the DSD approach has been developed and applied to hyperbolic systems or convection-dominated problems, this paper represents the first attempt, to our knowledge, to construct DSD schemes for the RTE. Our numerical results show that the DODSD method can lead to a more accurate solution in comparison with the DODG method.

The rest of this paper is organized as follows. In Section 2, we introduce the RTE and recall a few basic related results. In Section 3, we derive the discrete-ordinate discontinuous-streamline diffusion method, and in Section 4 we present a stability and convergence analysis for the proposed method. Numerical examples are presented in Section 5, illustrating the performance of the numerical method and providing numerical evidence of the theoretical error estimates. Finally, a few concluding remarks are given in Section 6.

Throughout this paper, standard notation is used for Sobolev spaces, and the corresponding semi-norms and norms [10]. Moreover, the letter C denotes a generic positive constant whose value may be different at different occurrences.

2. RADIATIVE TRANSFER EQUATION

Let X be a bounded domain in \mathbb{R}^d ($d = 2, 3$) with a smooth boundary ∂X . Denote by $\mathbf{n}(\mathbf{x})$ the unit outward normal for $\mathbf{x} \in \partial X$. Let Ω be the angular space, i.e., the unit circle in \mathbb{R}^2 , or the unit sphere in \mathbb{R}^3 . For each fixed direction $\boldsymbol{\omega} \in \Omega$, we introduce the following subsets of ∂X :

$$\partial X_{\boldsymbol{\omega},-} = \{\mathbf{x} \in \partial X : \boldsymbol{\omega} \cdot \mathbf{n}(\mathbf{x}) < 0\}, \quad \partial X_{\boldsymbol{\omega},+} = \{\mathbf{x} \in \partial X : \boldsymbol{\omega} \cdot \mathbf{n}(\mathbf{x}) \geq 0\}.$$

Then, we define

$$\Gamma_- = \{(\mathbf{x}, \boldsymbol{\omega}) : \mathbf{x} \in \partial X_{\boldsymbol{\omega}, -}, \boldsymbol{\omega} \in \Omega\}, \quad \Gamma_+ = \{(\mathbf{x}, \boldsymbol{\omega}) : \mathbf{x} \in \partial X_{\boldsymbol{\omega}, +}, \boldsymbol{\omega} \in \Omega\}$$

as the incoming and outgoing boundaries.

We define the integral operator S by

$$(Su)(\mathbf{x}, \boldsymbol{\omega}) = \int_{\Omega} g(\mathbf{x}, \boldsymbol{\omega} \cdot \hat{\boldsymbol{\omega}}) u(\mathbf{x}, \hat{\boldsymbol{\omega}}) d\sigma(\hat{\boldsymbol{\omega}}),$$

where g is a nonnegative normalized phase function satisfying

$$(2.1) \quad \int_{\Omega} g(\mathbf{x}, \boldsymbol{\omega} \cdot \hat{\boldsymbol{\omega}}) d\sigma(\hat{\boldsymbol{\omega}}) = 1 \quad \forall \mathbf{x} \in X, \boldsymbol{\omega} \in \Omega.$$

In most applications, the function g is independent of \mathbf{x} . As an example, a commonly used phase function is the following Henyey-Greenstein (H-G) function:

$$(2.2) \quad g(t) = \begin{cases} \frac{1-\eta^2}{2\pi(1+\eta^2-2\eta t)} & d=2, \\ \frac{1-\eta^2}{4\pi(1+\eta^2-2\eta t)^{3/2}} & d=3, \end{cases}$$

where the parameter $\eta \in (-1, 1)$ is the anisotropy factor of the scattering medium. Note that $\eta = 0$ for isotropic scattering, $\eta > 0$ for forward scattering, and $\eta < 0$ for backward scattering.

With the above notation, a boundary value problem of the radiative transfer equation (RTE) reads

$$(2.3) \quad \boldsymbol{\omega} \cdot \nabla u(\mathbf{x}, \boldsymbol{\omega}) + \sigma_t(\mathbf{x})u(\mathbf{x}, \boldsymbol{\omega}) = \sigma_s(\mathbf{x})(Su)(\mathbf{x}, \boldsymbol{\omega}) + f(\mathbf{x}, \boldsymbol{\omega}), \quad (\mathbf{x}, \boldsymbol{\omega}) \in X \times \Omega,$$

$$(2.4) \quad u(\mathbf{x}, \boldsymbol{\omega}) = 0, \quad (\mathbf{x}, \boldsymbol{\omega}) \in \Gamma_-.$$

Here $\sigma_t = \sigma_a + \sigma_s$, σ_a is the macroscopic absorption cross section, σ_s is the macroscopic scattering cross section, and f is a source function. We assume these given functions have the properties that

$$(2.5) \quad \sigma_t, \sigma_s \in L^\infty(X), \sigma_s \geq 0 \text{ a.e. in } X, \text{ and } \sigma_t - \sigma_s \geq c_0 \text{ in } X \text{ for a constant } c_0 > 0,$$

$$(2.6) \quad f(\mathbf{x}, \boldsymbol{\omega}) \in L^2(X \times \Omega) \text{ and is a continuous function with respect to } \boldsymbol{\omega} \in \Omega.$$

It is shown in [1] that the problem (2.3)–(2.4) has a unique solution $u \in H_2^1(X \times \Omega)$, where

$$H_2^1(X \times \Omega) := \{v \in L^2(X \times \Omega) : \boldsymbol{\omega} \cdot \nabla v \in L^2(X \times \Omega)\}$$

with $\boldsymbol{\omega} \cdot \nabla v$ denoting the generalized directional derivative of v in the direction $\boldsymbol{\omega}$.

3. A DISCRETE-ORDINATE DISCONTINUOUS-STREAMLINE DIFFUSION METHOD

In this section, a discrete-ordinate discontinuous-streamline diffusion method is presented for solving the radiative transfer problem (2.3)–(2.4). The numerical scheme is formed in two steps: First, we use the discrete-ordinate method to approximate the integral term in the RTE, resulting in a system of linear hyperbolic partial differential equations. Then these coupled linear hyperbolic equations are further discretized by the discontinuous-streamline diffusion method.

3.1. Angular discretization. To approximate the integration term Su , we employ a numerical quadrature of the form

$$(3.1) \quad \int_{\Omega} F(\boldsymbol{\omega}) d\sigma(\boldsymbol{\omega}) \approx \sum_{l=0}^L w_l F(\boldsymbol{\omega}_l), \quad w_l > 0, \quad \boldsymbol{\omega}_l \in \Omega, \quad 0 \leq l \leq L,$$

where F is a continuous function over the unit sphere Ω .

3.1.1. Quadrature scheme in the two-dimensional (2D) domain. Introduce the spherical coordinate system

$$(3.2) \quad \boldsymbol{\omega} = (\cos \theta, \sin \theta)^T, \quad 0 \leq \theta \leq 2\pi.$$

Noting that $d\sigma(\boldsymbol{\omega}) = d\theta$ holds for the coordinate system (3.2), we have

$$\int_{\Omega} F(\boldsymbol{\omega}) d\sigma(\boldsymbol{\omega}) = \int_0^{2\pi} \bar{F}(\theta) d\theta,$$

where \bar{F} stands for the representation of F in the spherical coordinates.

One possible quadrature scheme for the above integral is the composite trapezoidal formula

$$(3.3) \quad \int_0^{2\pi} \bar{F}(\theta) d\theta \approx \frac{h_\theta}{2} \left(\bar{F}(\theta_0) + \sum_{i=1}^{L-1} 2\bar{F}(\theta_i) + \bar{F}(\theta_L) \right) := \sum_{i=0}^L w_i \bar{F}(\theta_i),$$

where $\{\theta_i\}$ are evenly spaced on $[0, 2\pi]$ with a spacing $h_\theta = 2\pi/L$, i.e., $\theta_i = ih_\theta$, $w_0 = w_L = \frac{h_\theta}{2}$, and $w_i = h_\theta$ for $1 \leq i \leq L-1$. It is known that (see, e.g. [5])

$$(3.4) \quad \int_0^{2\pi} \bar{F}(\theta) d\theta - \frac{h_\theta}{2} \left(\bar{F}(\theta_0) + \sum_{i=1}^{L-1} 2\bar{F}(\theta_i) + \bar{F}(\theta_L) \right) = -\frac{\pi h_\theta^2}{6} \bar{F}''(\theta).$$

3.1.2. Quadrature scheme in the three-dimensional (3D) domain. Introduce the spherical coordinate system

$$(3.5) \quad \boldsymbol{\omega} = (\sin \theta \cos \psi, \sin \theta \sin \psi, \cos \theta)^T, \quad 0 \leq \theta \leq \pi, \quad 0 \leq \psi \leq 2\pi.$$

Then we have $d\sigma(\boldsymbol{\omega}) = \sin \theta d\theta d\psi$. By using the spherical coordinate system (3.5), we obtain

$$\int_{\Omega} F(\boldsymbol{\omega}) d\sigma(\boldsymbol{\omega}) = \int_0^{2\pi} \int_0^\pi \bar{F}(\theta, \psi) \sin \theta d\theta d\psi.$$

One family of quadratures for the above integral is given by the product numerical integration formulas. For example,

$$(3.6) \quad \int_{\Omega} F(\boldsymbol{\omega}) d\sigma(\boldsymbol{\omega}) \approx \frac{\pi}{m} \sum_{j=1}^{2m} \sum_{i=1}^m \bar{w}_i \bar{F}(\theta_i, \psi_j),$$

where $\{\theta_i\}$ are chosen so that $\{\cos \theta_i\}$ and $\{\bar{w}_i\}$ are the Gauss-Legendre nodes and weights on $[-1, 1]$. The points $\{\psi_j\}$ are evenly spaced on $[0, 2\pi]$ with a spacing of π/m . Regarding the accuracy of the quadrature (3.6), we have (see, e.g. [18])

$$(3.7) \quad \left| \int_{\Omega} F(\boldsymbol{\omega}) d\sigma(\boldsymbol{\omega}) - \sum_{l=0}^L w_l F(\boldsymbol{\omega}_l) \right| \leq c_s n^{-s} \|F\|_{s,\Omega} \quad \forall F \in H^s(\Omega), \quad s > 1,$$

where c_s is a positive constant depending only on s , and n denotes the degree of precision of the quadrature.

3.1.3. Discrete-ordinate method. Based on the numerical quadrature (3.1), the integral operator S is approximated by a discretized operator S_d given by

$$(3.8) \quad S_d u(\mathbf{x}, \boldsymbol{\omega}) = \sum_{i=0}^L w_i g(\mathbf{x}, \boldsymbol{\omega} \cdot \boldsymbol{\omega}_i) u(\mathbf{x}, \boldsymbol{\omega}_i).$$

For later analysis, we define

$$(3.9) \quad m(\mathbf{x}) = \max_{0 \leq l \leq L} \sum_{i=0}^L w_i g(\mathbf{x}, \boldsymbol{\omega}_l \cdot \boldsymbol{\omega}_i).$$

In the 2D case, if $g(\mathbf{x}, t)$ is continuous in $\mathbf{x} \in \bar{X}$ and twice continuously differentiable with respect to $t \in [-1, 1]$, then we get from (3.4) and (2.1) that

$$(3.10) \quad \left| 1 - \sum_{i=0}^L w_i g(\mathbf{x}, \boldsymbol{\omega}_l \cdot \boldsymbol{\omega}_i) \right| \leq O(h_{\theta}^2).$$

This implies

$$(3.11) \quad \|m(\mathbf{x})\|_{0,\infty,X} \leq 1 + O(h_{\theta}^2).$$

Therefore, for h_{θ} sufficiently small, there exists a positive constant c'_0 satisfying

$$(3.12) \quad \sigma_t - m(\mathbf{x})\sigma_s \geq \sigma_t - \sigma_s - O(h_{\theta}^2)\sigma_s \geq c_0 - O(h_{\theta}^2)\sigma_s \geq c'_0 \quad \forall \mathbf{x} \in X.$$

In the 3D case, if $g(\mathbf{x}, \boldsymbol{\omega}_l \cdot \cdot)$ is an $H^s(\Omega)$ ($s > 1$) function for any fixed $\mathbf{x} \in X$ and $\boldsymbol{\omega}_l \in \Omega$, then we get from (3.7) and (2.1) that

$$(3.13) \quad \left| 1 - \sum_{i=1}^L w_i g(\boldsymbol{\omega}_l \cdot \boldsymbol{\omega}_i) \right| \leq c_s n^{-s} \|g(\boldsymbol{\omega}_l \cdot \cdot)\|_{s,\Omega}.$$

This also implies that $\|m(\mathbf{x})\|_{0,\infty,X} \approx 1$ and (3.12) holds in the 3D case when a high-order quadrature rule is used.

Remark 3.1. Numerical tests are provided in [16] to demonstrate that (3.13) holds for the Henyey-Greenstein phase function (2.2).

Using the operator S_d , we can discretize the radiative transfer equation (2.3)–(2.4) in each angular direction ω_l to get

$$(3.14) \quad \omega_l \cdot \nabla u^l + \sigma_t u^l = \sigma_s \sum_{i=0}^L w_i g(\cdot, \omega_l \cdot \omega_i) u^i + f_l \quad \text{in } X, \quad u^l = 0 \text{ on } \partial_-^l X, \quad 0 \leq l \leq L,$$

where $f_l = f(\mathbf{x}, \omega_l)$ and $u^l = u^l(\mathbf{x})$ is an approximation of $u(\mathbf{x}, \omega_l)$. Here and below, we use the simplified notation $\partial_\pm^l X := \partial X_{\omega_l, \pm}$.

Remark 3.2. Note that the Henyey-Greenstein function (2.2) is smooth for $\eta < 1$. Formally, $\eta = 1$ corresponds to the case where there is no scattering among different directions and $(Su)(\mathbf{x}, \omega) = u(\mathbf{x}, \omega)$. As a result, the system (3.14) is reduced to a set of uncoupled first order transfer equations, which can be solved easily, and the analysis is the same as that for a single transfer equation.

3.2. Spatial discretization. After the angular discretization, the RTE is reduced to a system of first-order hyperbolic partial differential equations in space. Now we discretize (3.14) by the discontinuous-streamline diffusion method.

Let $\{T_h\}_h$ be a regular family of finite element partitions of X , h being the mesh size parameter. Denote by \mathbf{n}_K the unit outward normal to ∂K for $K \in T_h$. Let E_h^i be the set of all interior boundaries (faces for $d = 3$ or edges for $d = 2$) of T_h . For any positive integer k , let $P_k(K)$ be the set of all polynomials on K of a total degree no more than k .

For a fixed direction ω_l , we define the incoming and outgoing boundaries of $K \in T_h$ by

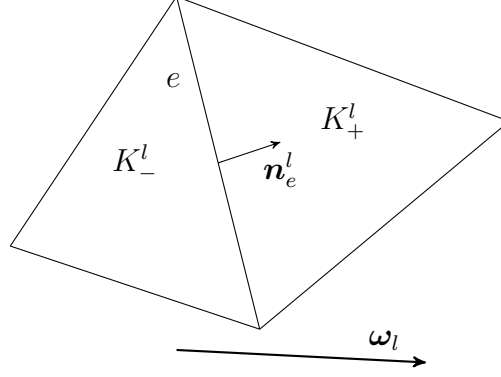
$$\partial_-^l K = \{\mathbf{x} \in \partial K : \omega_l \cdot \mathbf{n}(\mathbf{x}) < 0\}, \quad \partial_+^l K = \{\mathbf{x} \in \partial K : \omega_l \cdot \mathbf{n}(\mathbf{x}) \geq 0\}.$$

We remark that each edge of an element $K \in T_h$ is either an incoming boundary or an outgoing boundary.

Let K_+^l and K_-^l be two adjacent elements sharing $e \in E_h^i$, where the normal direction \mathbf{n}_e^l pointing from K_-^l to K_+^l satisfies $\omega \cdot \mathbf{n}_e^l \geq 0$ (cf. Figure 1). For a scalar-valued function v , we define

$$v_+^l = v|_{K_+^l}, \quad v_-^l = v|_{K_-^l}, \quad \text{and } [v^l] = v_+^l - v_-^l \quad \text{on } e.$$

For any domain $D \subseteq X$ with boundary ∂D (resp. $\partial_\pm^l D$), let $(\cdot, \cdot)_D$ and $\langle \cdot, \cdot \rangle_{\partial D}$ (resp. $\langle \cdot, \cdot \rangle_{\partial_\pm^l D}$) be the L^2 inner product on D and on ∂D (resp. $\partial_\pm^l D$).

FIGURE 1. An example of K_-^l , K_+^l , and \mathbf{n}_e^l in 2D

Using the above notation, the DODG method, which has been developed in [16], is to find $u_h^l \in P_k(K)$ such that for any $K \in T_h$, $0 \leq l \leq L$,

$$(3.15) \quad \begin{aligned} & \left(\omega_l \cdot \nabla u_h^l + \sigma_t u_h^l, v_h^l \right)_K + \left\langle [u_h^l], v_+^l | \omega_l \cdot \mathbf{n} | \right\rangle_{\partial_-^l K} \\ &= \left(\sigma_s \sum_{i=0}^L w_i g(\cdot, \omega_l \cdot \omega_i) u_h^i + f_l, v_h^l \right)_K \quad \forall v_h^l \in P_k(K) \end{aligned}$$

with

$$(3.16) \quad u_-^l = 0 \quad \text{on } \partial_-^l K \subset \partial_-^l X.$$

We now replace the Galerkin elements in the above DODG formulation (3.15) by the SD framework, and add an artificial diffusion term in the test function. Then the discrete-ordinate discontinuous-streamline diffusion (DODSD) method can be described as follows: to find $u_h^l \in P_k(K)$ such that for any $K \in T_h$, $0 \leq l \leq L$,

$$(3.17) \quad \begin{aligned} & \left(\omega_l \cdot \nabla u_h^l + \sigma_t u_h^l, v_h^l + \delta \omega_l \cdot \nabla v_h^l \right)_K + \left\langle [u_h^l], v_+^l | \omega_l \cdot \mathbf{n} | \right\rangle_{\partial_-^l K} \\ &= \left(\sigma_s \sum_{i=0}^L w_i g(\cdot, \omega_l \cdot \omega_i) u_h^i + f_l, v_h^l + \delta \omega_l \cdot \nabla v_h^l \right)_K \quad \forall v_h^l \in P_k(K) \end{aligned}$$

with

$$(3.18) \quad u_-^l = 0 \quad \text{on } \partial_-^l K \subset \partial_-^l X.$$

Here $\delta = \bar{c}h$ is an artificial diffusion parameter with some $\bar{c} > 0$ and $v_\pm^l := (v_h^l)_\pm$.

Obviously, the DODG method is the special case of the DODSD method with $\delta = 0$. The effect of adding the diffusion parameter will be analyzed in the next section, and illustrated by some numerical results in Section 5.2.

4. ERROR ANALYSIS

In order to analyze the proposed DODSD method, we first present the global formulation of the discrete method (3.17)–(3.16). Associated with a direction $\boldsymbol{\omega}_l$, we define

$$(4.1) \quad V_h^l = \{v \in L^2(X) : v|_K \in P_k(K) \ \forall K \in T_h\},$$

$$(4.2) \quad W_h^l = \{w \in L^2(X) : w|_K \in C(K) \cap H^1(K) \ \forall K \in T_h\}.$$

Letting $\mathbf{V}_h = (V_h^l)^{L+1}$ and $\mathbf{W}_h := (W_h^l)^{L+1}$, we have $\mathbf{V}_h \subset \mathbf{W}_h$. A generic element in \mathbf{V}_h will be denoted by $\mathbf{v}_h := \{v_h^l\}_{l=0}^L$ or simply $\mathbf{v}_h := \{v_h^l\}$.

The global formulation of the DODSD method (3.17)–(3.16) is then expressed as: Find $\{u_h^l\} \in \mathbf{V}_h$ such that

$$(4.3) \quad \begin{aligned} & \sum_{l=0}^L w_l \sum_{K \in T_h} \left(\boldsymbol{\omega}_l \cdot \nabla u_h^l + \sigma_t u_h^l, v_h^l + \delta \boldsymbol{\omega}_l \cdot \nabla v_h^l \right)_K + \sum_{l=0}^L w_l \sum_{K \in T_h} \left\langle [u_h^l], v_h^l | \boldsymbol{\omega}_l \cdot \mathbf{n} \right\rangle_{\partial_-^l K} \\ &= \sum_{l=0}^L w_l \sum_{K \in T_h} \left(\sigma_s \sum_{i=0}^L w_i g(\cdot, \boldsymbol{\omega}_l \cdot \boldsymbol{\omega}_i) u_h^i + f_l, v_h^l + \delta \boldsymbol{\omega}_l \cdot \nabla v_h^l \right)_K \quad \forall \{v_h^l\} \in \mathbf{V}_h \end{aligned}$$

with

$$(4.4) \quad u_-^l = 0 \quad \text{on } \partial_-^l K \subset \partial_-^l X, \ 0 \leq l \leq L.$$

We define a bilinear form $a_h : \mathbf{W}_h \times \mathbf{W}_h \rightarrow \mathbb{R}$ as

$$\begin{aligned} a_h(\mathbf{u}_h, \mathbf{v}_h) &= \sum_{l=0}^L w_l \sum_{K \in T_h} \left(\boldsymbol{\omega}_l \cdot \nabla u_h^l + \sigma_t u_h^l, v_h^l + \delta \boldsymbol{\omega}_l \cdot \nabla v_h^l \right)_K \\ &\quad + \sum_{l=0}^L w_l \sum_{K \in T_h} \left\langle [u_h^l], v_h^l | \boldsymbol{\omega}_l \cdot \mathbf{n} \right\rangle_{\partial_-^l K} \\ &\quad - \sum_{l=0}^L w_l \sum_{K \in T_h} \left(\sigma_s \sum_{i=0}^L w_i g(\cdot, \boldsymbol{\omega}_l \cdot \boldsymbol{\omega}_i) u_h^i, v_h^l + \delta \boldsymbol{\omega}_l \cdot \nabla v_h^l \right)_K \end{aligned}$$

and a linear form $f : \mathbf{W}_h \rightarrow \mathbb{R}$ by

$$f(\mathbf{v}_h) = \sum_{l=0}^L w_l \sum_{K \in T_h} \left(f_l, v_h^l + \delta \boldsymbol{\omega}_l \cdot \nabla v_h^l \right)_K.$$

Then we rewrite the DODSD method for the problem (2.3)–(2.4): Find $\mathbf{u}_h \in \mathbf{V}_h$ such that

$$(4.5) \quad a_h(\mathbf{u}_h, \mathbf{v}_h) = f(\mathbf{v}_h) \quad \forall \mathbf{v}_h \in \mathbf{V}_h,$$

with

$$(4.6) \quad [u_h^l] = u_+^l \quad \text{on } \partial_-^l K \subset \partial_-^l X, \ 0 \leq l \leq L.$$

4.1. Stability and unique solvability. We begin with a useful lemma.

Lemma 4.1. *For any $\mathbf{v}_h = \{v_h^l\}$, $\mathbf{w}_h = \{w_h^l\} \in (L^2(\Omega))^{L+1}$, we have*

$$\begin{aligned} & \sum_{l=0}^L w_l \left(\sigma_s \sum_{i=0}^L w_i g(\cdot, \boldsymbol{\omega}_l \cdot \boldsymbol{\omega}_i) v_h^i, w_h^l \right)_X \\ & \leq \left[\sum_{l=0}^L w_l \left(m \sigma_s v_h^l, v_h^l \right)_X \right]^{\frac{1}{2}} \left[\sum_{l=0}^L w_l \left(m \sigma_s w_h^l, w_h^l \right)_X \right]^{\frac{1}{2}}. \end{aligned}$$

Proof. Interchanging the order of summation, we have

$$I := \sum_{l=0}^L w_l \left(\sigma_s \sum_{i=0}^L w_i g(\cdot, \boldsymbol{\omega}_l \cdot \boldsymbol{\omega}_i) v_h^i, w_h^l \right)_X = \sum_{i=0}^L w_i \sum_{l=0}^L \left(\sigma_s w_l g(\cdot, \boldsymbol{\omega}_l \cdot \boldsymbol{\omega}_i) v_h^i, w_h^l \right)_X.$$

Using the Cauchy-Schwarz inequality, we get

$$(4.7) \quad I \leq \sum_{i=0}^L w_i \left[\sum_{l=0}^L \left(\sigma_s w_l g(\cdot, \boldsymbol{\omega}_l \cdot \boldsymbol{\omega}_i) v_h^i, v_h^i \right)_X \right]^{\frac{1}{2}} \left[\sum_{l=0}^L \left(\sigma_s w_l g(\cdot, \boldsymbol{\omega}_l \cdot \boldsymbol{\omega}_i) w_h^l, w_h^l \right)_X \right]^{\frac{1}{2}}.$$

It follows from the definition (3.9) that

$$\sum_{l=0}^L \left(\sigma_s w_l g(\cdot, \boldsymbol{\omega}_l \cdot \boldsymbol{\omega}_i) v_h^i, v_h^i \right)_X \leq (m \sigma_s v_h^i, v_h^i)_X.$$

Therefore, a combination of the inequality (4.7) and the Cauchy-Schwarz inequality leads to

$$\begin{aligned} I & \leq \sum_{i=0}^L w_i \left[(m \sigma_s v_h^i, v_h^i)_X \right]^{\frac{1}{2}} \left[\sum_{l=0}^L \left(\sigma_s w_l g(\cdot, \boldsymbol{\omega}_l \cdot \boldsymbol{\omega}_i) w_h^l, w_h^l \right)_X \right]^{\frac{1}{2}} \\ & \leq \left[\sum_{i=0}^L w_i (m \sigma_s v_h^i, v_h^i)_X \right]^{\frac{1}{2}} \left[\sum_{i=0}^L w_i \sum_{l=0}^L \left(\sigma_s w_l g(\cdot, \boldsymbol{\omega}_l \cdot \boldsymbol{\omega}_i) w_h^l, w_h^l \right)_X \right]^{\frac{1}{2}} \\ & \leq \left[\sum_{i=0}^L w_i (m \sigma_s v_h^i, v_h^l)_X \right]^{\frac{1}{2}} \left[\sum_{l=0}^L w_l (m \sigma_s w_h^i, w_h^l)_X \right]^{\frac{1}{2}}, \end{aligned}$$

which completes the proof of the lemma. \square

For any $\mathbf{v}_h \in \mathbf{W}_h$, we define a norm $||| \cdot |||$ by

$$\begin{aligned} ||| \mathbf{v}_h |||^2 & = \sum_{l=0}^L w_l \sum_{K \in T_h} c_0 \|v_h^l\|_{0,K}^2 + \sum_{l=0}^L w_l \sum_{\partial_+^l K \subset \partial_+^l X} \left\langle v_-^l, v_-^l \boldsymbol{\omega}_l \cdot \mathbf{n} \right\rangle_{\partial_+^l K} \\ & \quad + \delta \sum_{l=0}^L w_l \sum_{K \in T_h} \|\boldsymbol{\omega}_l \cdot \nabla v_h^l\|_{0,K}^2 + \sum_{l=0}^L w_l \sum_{K \in T_h} \left\langle [v_h^l], [v_h^l] |\boldsymbol{\omega}_l \cdot \mathbf{n}| \right\rangle_{\partial_-^l K}. \end{aligned}$$

We remark that $[v_h^l] = v_+^l$ on $\partial_-^l K \subset \partial_-^l X$, $l = 0, \dots, L$.

Then we prove a stability estimate for the method (4.5)–(4.6).

Lemma 4.2. *For sufficiently small h , we have*

$$|||\mathbf{v}_h|||^2 \leq 3a_h(\mathbf{v}_h, \mathbf{v}_h) \quad \forall \mathbf{v}_h \in \mathbf{W}_h.$$

Proof. Noting that $\boldsymbol{\omega}_l$ is a constant vector, we get from the Green formula that

$$(4.8) \quad (\boldsymbol{\omega}_l \cdot \nabla v_h, v_h)_K = -(v_h, \boldsymbol{\omega}_l \cdot \nabla v_h)_K + \langle v_h, v_h \boldsymbol{\omega}_l \cdot \mathbf{n} \rangle_{\partial K} = \frac{1}{2} \langle v_h, v_h \boldsymbol{\omega}_l \cdot \mathbf{n} \rangle_{\partial K}.$$

Thus,

$$a_h(\mathbf{v}_h, \mathbf{v}_h) = \sum_{l=0}^L w_l \sum_{K \in T_h} \delta \|\boldsymbol{\omega}_l \cdot \nabla v_h^l\|_{0,K}^2 + \sum_{l=0}^L w_l \sum_{K \in T_h} (\sigma_t v_h^l, v_h^l)_K + I_1 + I_2 + I_3 + I_4,$$

where

$$\begin{aligned} I_1 &= \sum_{l=0}^L w_l \sum_{K \in T_h} (\delta \sigma_t v_h^l, \boldsymbol{\omega}_l \cdot \nabla v_h^l)_K, \\ I_2 &= \sum_{l=0}^L w_l \sum_{K \in T_h} \left(\frac{1}{2} \langle v_h^l, v_h^l \boldsymbol{\omega}_l \cdot \mathbf{n} \rangle_{\partial K} + \langle [v_h^l], v_+^l |\boldsymbol{\omega}_l \cdot \mathbf{n}| \rangle_{\partial_-^l K} \right), \\ I_3 &= - \sum_{l=0}^L w_l \sum_{K \in T_h} \left(\sigma_s \sum_{i=0}^L w_i g(\cdot, \boldsymbol{\omega}_l \cdot \boldsymbol{\omega}_i) v_h^i, v_h^l \right)_K, \\ I_4 &= - \sum_{l=0}^L w_l \sum_{K \in T_h} \left(\sigma_s \sum_{i=0}^L w_i g(\cdot, \boldsymbol{\omega}_l \cdot \boldsymbol{\omega}_i) v_h^i, \delta \boldsymbol{\omega}_l \cdot \nabla v_h^l \right)_K. \end{aligned}$$

By the Cauchy-Schwarz inequality, we get

$$\begin{aligned} |I_1| &\leq \left[\sum_{l=0}^L w_l \sum_{K \in T_h} (\delta \sigma_t v_h^l, \sigma_t v_h^l)_K \right]^{\frac{1}{2}} \left[\sum_{l=0}^L w_l \sum_{K \in T_h} (\delta \boldsymbol{\omega}_l \cdot \nabla v_h^l, \boldsymbol{\omega}_l \cdot \nabla v_h^l)_K \right]^{\frac{1}{2}} \\ &\leq \frac{1}{2} \delta \sum_{l=0}^L w_l \sum_{K \in T_h} (\sigma_t v_h^l, \sigma_t v_h^l)_K + \frac{1}{2} \sum_{l=0}^L w_l \sum_{K \in T_h} (\delta \boldsymbol{\omega}_l \cdot \nabla v_h^l, \boldsymbol{\omega}_l \cdot \nabla v_h^l)_K. \end{aligned}$$

A simple calculation yields

$$\begin{aligned} I_2 &= \sum_{l=0}^L w_l \sum_{K \in T_h} \left(-\frac{1}{2} \langle v_+^l, v_+^l |\boldsymbol{\omega}_l \cdot \mathbf{n}| \rangle_{\partial_-^l K} + \frac{1}{2} \langle v_-^l, v_-^l \boldsymbol{\omega}_l \cdot \mathbf{n} \rangle_{\partial_+^l K} + \langle [v_h^l], v_+^l |\boldsymbol{\omega}_l \cdot \mathbf{n}| \rangle_{\partial_-^l K} \right) \\ &= \sum_{l=0}^L w_l \sum_{K \in T_h} \left(-\frac{1}{2} \langle v_+^l, v_+^l |\boldsymbol{\omega}_l \cdot \mathbf{n}| \rangle_{\partial_-^l K} + \frac{1}{2} \langle v_-^l, v_-^l |\boldsymbol{\omega}_l \cdot \mathbf{n}| \rangle_{\partial_-^l K} + \langle [v_h^l], v_+^l |\boldsymbol{\omega}_l \cdot \mathbf{n}| \rangle_{\partial_-^l K} \right) \\ &\quad + \sum_{l=0}^L w_l \sum_{\partial_+^l K \subset \partial_+^l X} \frac{1}{2} \langle v_-^l, v_-^l |\boldsymbol{\omega}_l \cdot \mathbf{n}| \rangle_{\partial_+^l K} \\ &= \sum_{l=0}^L w_l \sum_{K \in T_h} \left(\frac{1}{2} \langle [v_h^l], [v_h^l] |\boldsymbol{\omega}_l \cdot \mathbf{n}| \rangle_{\partial_-^l K} \right) + \sum_{l=0}^L w_l \sum_{\partial_+^l K \subset \partial_+^l X} \frac{1}{2} \langle v_-^l, v_-^l |\boldsymbol{\omega}_l \cdot \mathbf{n}| \rangle_{\partial_+^l K}, \end{aligned}$$

where the condition that $v_-^l = 0$ on $\partial_-^l K \subset \partial_-^l X$ is used.

Using Lemma 4.1, we get

$$|I_3| \leq \sum_{l=0}^L w_l \sum_{K \in T_h} \left(m \sigma_s v_h^l, v_h^l \right)_K$$

and

$$\begin{aligned} |I_4| &\leq \left[\sum_{l=0}^L w_l \sum_{K \in T_h} \left(m \sigma_s v_h^l, v_h^l \right)_K \right]^{\frac{1}{2}} \left[\sum_{l=0}^L w_l \sum_{K \in T_h} \left(m \sigma_s \delta^2 \boldsymbol{\omega}_l \cdot \nabla v_h^l, \boldsymbol{\omega}_l \cdot \nabla v_h^l \right)_K \right]^{\frac{1}{2}} \\ &\leq \frac{1}{2} \delta^{\frac{2}{3}} \sum_{l=0}^L w_l \sum_{K \in T_h} \left(m \sigma_s v_h^l, v_h^l \right)_K + \frac{1}{2} \delta^{\frac{4}{3}} \sum_{l=0}^L w_l \sum_{K \in T_h} \left(m \sigma_s \boldsymbol{\omega}_l \cdot \nabla v_h^l, \boldsymbol{\omega}_l \cdot \nabla v_h^l \right)_K. \end{aligned}$$

Combining the above inequalities, we have

$$\begin{aligned} a_h(\mathbf{v}_h, \mathbf{v}_h) &\geq \sum_{l=0}^L w_l \sum_{K \in T_h} \left(\frac{1}{2} \delta \left(1 - \delta^{\frac{1}{3}} m \sigma_s \right) \boldsymbol{\omega}_l \cdot \nabla v_h^l, \boldsymbol{\omega}_l \cdot \nabla v_h^l \right)_K \\ &\quad + \sum_{l=0}^L w_l \sum_{K \in T_h} \left(\left(\sigma_t - \frac{1}{2} \delta \sigma_t^2 - (1 + \delta^{\frac{2}{3}}) m \sigma_s \right) v_h^l, v_h^l \right)_K \\ &\quad + \sum_{l=0}^L w_l \sum_{K \in T_h} \left(\frac{1}{2} \left\langle [v_h^l], [v_h^l] \mid \boldsymbol{\omega}_l \cdot \mathbf{n} \right\rangle_{\partial_-^l K} \right) + \sum_{l=0}^L w_l \sum_{\partial_+^l K \in \partial_+^l X} \frac{1}{2} \left\langle v_-^l, v_-^l \mid \boldsymbol{\omega}_l \cdot \mathbf{n} \right\rangle_{\partial_+^l K}. \end{aligned}$$

Then the lemma can be obtained by taking a sufficiently small h . \square

The unique solvability of the method (4.5)–(4.6) is a direct consequence of the above lemma.

Theorem 4.3. *For sufficiently small h , the DODSD method (4.3) has a unique solution.*

4.2. Error estimate. For any $K \in T_h$, let P_K be the orthogonal projection operator from $L^2(K)$ onto $P_k(K)$. Then by the scaling argument and the trace theorem we can easily obtain the following result (cf. [7]).

Lemma 4.4. *For all $v \in H^{1+r}(K)$ with $r > 0$ and $K \in T_h$, we have*

$$\|v - P_K v\|_{0,K} + h_K \|v - P_K v\|_{1,K} + h_K^{\frac{1}{2}} \|v - P_K v\|_{0,\partial K} \leq C h_K^{1+\min\{r,k\}} \|v\|_{r+1,K}.$$

For later analysis, we make a regularity assumption:

$$(4.9) \quad \text{for some } r > 0, \ u^l \in H^{1+r}(X) \cap C(\overline{X}), \ 0 \leq l \leq L.$$

Theorem 4.5. *Let $\{u^l\}$ and \mathbf{u}_h be the solutions of (3.14) and (4.5)–(4.6), respectively. Under assumptions (2.5) and (4.9), we have, for all sufficiently small h ,*

$$(4.10) \quad |||\{u^l\} - \mathbf{u}_h||| \leq C_1 h^{\min\{r,k\} + \frac{1}{2}} \left(\sum_{l=0}^L \|u^l\|_{r+1,X} \right)^{\frac{1}{2}}.$$

Proof. By the regularity assumption (4.9), we have

$$(4.11) \quad a_h \left(\{u^l\}, \{v_h^l\} \right) = 0 \quad \forall \{v_h^l\} \in \mathbf{V}_h.$$

Subtracting the above equality from (4.5), we obtain the Galerkin orthogonality

$$(4.12) \quad a_h \left(\{u^l\} - \mathbf{u}_h, \{v_h^l\} \right) = 0 \quad \forall \{v_h^l\} \in \mathbf{V}_h.$$

Let P_h denote the L^2 -orthogonal operator onto V_h^l , $0 \leq l \leq L$, in an elementwise way, i.e., for $v \in L^2(X)$, let

$$P_h v|_K := P_K v \quad \forall K \in T_h.$$

Set

$$\eta^l = u^l - P_h u^l, \quad \xi^l = P_h u^l - u_h^l, \quad \text{and} \quad e^l = u^l - u_h^l.$$

Note that $e_-^l|_{\partial_-^l K} = 0$ for each $\partial_-^l K \subset \partial_-^l X$.

From Lemma 4.2 and the Galerkin orthogonality (4.12), we have

$$(4.13) \quad |||\{e^l\}|||^2 \leq 3a_h \left(\{e^l\}, \{e^l\} \right) = 3a_h \left(\{e^l\}, \{\eta^l\} \right).$$

On the other hand, by the definition of the bilinear form $a_h(\cdot, \cdot)$, we have

$$(4.14) \quad a_h \left(\{e^l\}, \{\eta^l\} \right) = I_1 + I_2 + I_3 + I_4 + I_5,$$

where

$$\begin{aligned} I_1 &= \sum_{l=0}^L w_l \sum_{K \in T_h} \left(\boldsymbol{\omega}_l \cdot \nabla e^l, \eta^l \right)_K, \\ I_2 &= \sum_{l=0}^L w_l \sum_{K \in T_h} \delta \left(\boldsymbol{\omega}_l \cdot \nabla e^l, \boldsymbol{\omega}_l \cdot \nabla \eta^l \right)_K, \\ I_3 &= \sum_{l=0}^L w_l \sum_{K \in T_h} \left(\sigma_t e^l, \eta^l + \delta \boldsymbol{\omega}_l \cdot \nabla \eta^l \right)_K \\ I_4 &= \sum_{l=0}^L w_l \sum_{K \in T_h} \left(\sigma_s \sum_{i=0}^L w_i g(\mathbf{x}, \boldsymbol{\omega}_l \cdot \boldsymbol{\omega}_i) e^i, \eta^l + \delta \boldsymbol{\omega}_l \cdot \nabla \eta^l \right)_K, \\ I_5 &= \sum_{l=0}^L w_l \sum_{K \in T_h} \left\langle [e^l], \eta_+^l | \boldsymbol{\omega}_l \cdot \mathbf{n} | \right\rangle_{\partial_-^l K}. \end{aligned}$$

By using the Cauchy-Schwarz inequality, Young's inequality, and Lemma 4.4, we get

$$\begin{aligned}
 (4.15) \quad |I_1| &\leq \sum_{l=0}^L w_l \sum_{K \in T_h} \|\boldsymbol{\omega}_l \cdot \nabla e^l\|_{0,K} \|\eta^l\|_{0,K} \\
 &\leq \sum_{l=0}^L w_l \sum_{K \in T_h} C h_K^{1+\min\{r,k\}} \|\boldsymbol{\omega}_l \cdot \nabla e^l\|_{0,K} \|u^l\|_{r+1,K} \\
 &\leq \sum_{l=0}^L w_l \sum_{K \in T_h} \left(\frac{1}{6} \delta \|\boldsymbol{\omega}_l \cdot \nabla e^l\|_{0,K}^2 + C h_K^{2+2\min\{r,k\}} \delta^{-1} \|u^l\|_{r+1,K}^2 \right),
 \end{aligned}$$

$$\begin{aligned}
 (4.16) \quad |I_2| &\leq \sum_{l=0}^L w_l \sum_{K \in T_h} \left(\delta \|\boldsymbol{\omega}_l \cdot \nabla e^l\|_{0,K} \|\boldsymbol{\omega}_l \cdot \nabla \eta^l\|_{0,K} \right) \\
 &\leq \sum_{l=0}^L w_l \sum_{K \in T_h} \delta h_K^{\min\{r,k\}} \|\boldsymbol{\omega}_l \cdot \nabla e^l\|_{0,K} \|u^l\|_{r+1,K} \\
 &\leq \sum_{l=0}^L w_l \sum_{K \in T_h} \left(\frac{1}{6} \delta \|\boldsymbol{\omega}_l \cdot \nabla e^l\|_{0,K}^2 + C h_K^{2\min\{r,k\}} \delta \|u^l\|_{r+1,K}^2 \right),
 \end{aligned}$$

$$\begin{aligned}
 (4.17) \quad |I_3| &\leq \sum_{l=0}^L w_l \sum_{K \in T_h} \left(\|\sigma_t e^l\|_{0,K} \|\eta^l\| + \delta \|\boldsymbol{\omega}_l \cdot \nabla \eta^l\|_{0,K} \right) \\
 &\leq \sum_{l=0}^L w_l \sum_{K \in T_h} \left(\frac{1}{6} c'_0 \|e^l\|_{0,K}^2 + C \left(\|\eta^l\|_{0,K}^2 + \delta \|\boldsymbol{\omega}_l \cdot \nabla \eta^l\|_{0,K}^2 \right) \right) \\
 &\leq \sum_{l=0}^L w_l \sum_{K \in T_h} \left(\frac{1}{6} c'_0 \|e^l\|_{0,K}^2 + C \left(h_K^{2+2\min\{r,k\}} \|u^l\|_{r+1,K}^2 + \delta h_K^{2\min\{r,k\}} \|u^l\|_{r+1,K}^2 \right) \right),
 \end{aligned}$$

$$\begin{aligned}
 (4.18) \quad |I_4| &\leq C \left[\sum_{l=0}^L w_l \sum_{K \in T_h} \|e^l\|_{0,K}^2 \right]^{\frac{1}{2}} \left[\sum_{l=0}^L w_l \sum_{K \in T_h} \|\eta^l + \delta \boldsymbol{\omega}_l \cdot \nabla \eta^l\|_{0,K}^2 \right]^{\frac{1}{2}} \\
 &\leq \sum_{l=0}^L w_l \sum_{K \in T_h} \frac{1}{6} c'_0 \|e^l\|_{0,K}^2 + C \sum_{l=0}^L w_l \sum_{K \in T_h} \left(\|\eta^l\|_{0,K}^2 + \delta \|\boldsymbol{\omega}_l \cdot \nabla \eta^l\|_{0,K}^2 \right) \\
 &\leq \sum_{l=0}^L w_l \sum_{K \in T_h} \frac{1}{6} c'_0 \|e^l\|_{0,K}^2 + C \sum_{l=0}^L w_l \sum_{K \in T_h} \left(h_K^{2+2\min\{r,k\}} \|u^l\|_{r+1,K}^2 + \delta h_K^{2\min\{r,k\}} \|u^l\|_{r+1,K}^2 \right)
 \end{aligned}$$

and

$$\begin{aligned}
 (4.19) \quad |I_5| &\leq \sum_{l=0}^L w_l \sum_{K \in T_h} \left(\frac{1}{6} \left\langle [e^l], [e^l] |\boldsymbol{\omega}_l \cdot \mathbf{n}| \right\rangle_{\partial_-^l K} + C \left\langle \eta_+^l, \eta_+^l |\boldsymbol{\omega}_l \cdot \mathbf{n}| \right\rangle_{\partial_-^l K} \right) \\
 &\leq \sum_{l=0}^L w_l \sum_{K \in T_h} \left(\frac{1}{6} \left\langle [e^l], [e^l] |\boldsymbol{\omega}_l \cdot \mathbf{n}| \right\rangle_{\partial_-^l K} + C h_K^{1+2\min\{r,k\}} \|u^l\|_{r+1,K}^2 \right).
 \end{aligned}$$

Combining (4.13)–(4.19), we obtain

$$(4.20) \quad |||\{e^l\}|||^2 \leq \frac{1}{2} |||\{e^l\}|||^2 + Ch_K^{1+2\min\{r,k\}} \sum_{l=0}^L w_l \sum_{K \in T_h} \|u^l\|_{r+1,K}^2,$$

where $\delta = \bar{c}h$ is used. Thus we complete the proof of this theorem. \square

Remark 4.6. Note that $\|\omega_l \cdot \nabla(u^l - u_h^l)\|_{0,K}$ is included in the norm $|||\{u^l\} - \mathbf{u}_h|||$, therefore (4.10) also gives a stability estimate for $\|\omega_l \cdot \nabla(u^l - u_h^l)\|_{0,K}$ in terms of $\|u^l\|_{r+1,X}$. We remark that this estimate was not established for the DODG approximation solution of the RTE, cf. Theorem 4.6 in [16].

Error estimates between the solution u to the RTE and the solution $\{u^l\}$ to the semi-discretized equation (3.14) have been proved in [16].

Theorem 4.7. Let $\{u^l\}$ and u be the solutions of (3.14) and (2.3)–(2.4), respectively. In 3D, if the regularity assumption (4.9) holds, then we have

$$(4.21) \quad \left(\sum_{l=0}^l w_l \sum_{K \in T_h} \|u^l(\cdot) - u(\cdot, \omega_l)\|_{0,K}^2 \right)^{\frac{1}{2}} \leq C_2 n^{-r-1} \left(\int_X \|u(\cdot, \cdot)\|_{r+1,\Omega}^2 d\mathbf{x} \right)^{\frac{1}{2}},$$

where C_1 is positive constant depending on r and the phase function g .

Similarly, we can obtain the following theorem.

Theorem 4.8. Let $\{u^l\}$ and u be the solutions of (3.14) and (2.3)–(2.4), respectively. In 2D, if the solution u to RTE (2.3)–(2.4) is in $L^2(X, C^2(\Omega))$ and there exists a positive constant C such that

$$(4.22) \quad \sup_{\mathbf{x} \in X, \omega \in \Omega} \|g''(\mathbf{x}, \omega \cdot)\|_{0,\infty,\Omega} \leq C,$$

where $g''(\mathbf{x}, t) = \frac{\partial^2 g(\mathbf{x}, t)}{\partial t^2}$, then we have

$$(4.23) \quad \left(\sum_{l=0}^l w_l \sum_{K \in T_h} \|u^l(\cdot) - u(\cdot, \omega_l)\|_{0,K}^2 \right)^{\frac{1}{2}} = O(h_\theta^2),$$

when h_θ is sufficiently small.

Combining the above three theorems, we obtain the following results.

Theorem 4.9. Let \mathbf{u}_h and u be the solutions of (4.5)–(4.6) and (2.3)–(2.4), respectively. Under the assumption of Theorem 4.7, we have

$$(4.24) \quad \left(\sum_{l=0}^l w_l \sum_{K \in T_h} \|u_h^l(\cdot) - u(\cdot, \omega_l)\|_{0,K}^2 \right)^{\frac{1}{2}} \leq C_1 h^{\min\{r,k\}+\frac{1}{2}} \left(\sum_{l=0}^L w_l \sum_{K \in T_h} \|u^l\|_{r+1,K}^2 \right)^{\frac{1}{2}} \\ + C_2 n^{-r-1} \left(\int_X \|u(\cdot, \cdot)\|_{r+1,\Omega}^2 d\mathbf{x} \right)^{\frac{1}{2}},$$

when h is sufficiently small.

Theorem 4.10. Let \mathbf{u}_h and u be the solutions of (4.5)–(4.6) and (2.3)–(2.4), respectively. Under the assumption of Theorem 4.8, we have

$$(4.25) \quad \left(\sum_{l=0}^L w_l \sum_{K \in T_h} \left\| u_h^l(\cdot) - u(\cdot, \omega_l) \right\|_{0,K}^2 \right)^{\frac{1}{2}} \leq C_1 h^{\min\{r,k\} + \frac{1}{2}} \left(\sum_{l=0}^L w_l \sum_{K \in T_h} \|u^l\|_{r+1,K}^2 \right)^{\frac{1}{2}} + O(h_\theta^2),$$

when h is sufficiently small.

5. NUMERICAL EXPERIMENTS

In this section, we present some numerical examples of the discrete-ordinate discontinuous-streamline diffusion method for the radiative transfer equation (2.3)–(2.4) in the 2D case. The main purpose is to illustrate the convergence performance of the proposed DODSD method and the effect of the added diffusion parameter.

5.1. Implementation. First, we briefly describe the implementation of the DODSD method. For a mesh shown in Figure 2, the DODSD method can be carried out for one direction ω in the following order:

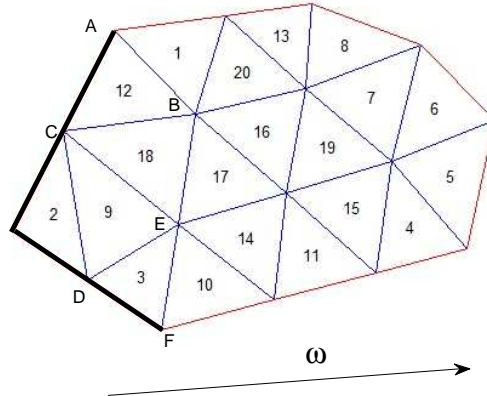


FIGURE 2. A example of T_h in 2D

Step 1. Denote by $T_h^{(1)}$ the elements for which all incoming boundary $\partial_-^l K \subset \partial_-^l X$. In Figure 2, $T_h^{(1)} = \{K_i : i = 2, 3\}$. We first compute u_h^l for $K \in T_h^{(1)}$.

Step 2. For $T_h \setminus T_h^{(1)}$, let $\partial_-^{l,1} X = \{e \subset \partial_-^l K : K \in T_h \setminus T_h^{(1)}, \text{ and } u_+^l|_e \text{ has been computed or given}\}$ denote its incoming edge. In Figure 2, $\partial_-^{l,1}$ is the broken line \overline{ACDEF} . Similarly, we define the set $T_h^{(2)}$ and compute u_h^l for $K \in T_h^{(2)}$. In Figure 2, $T_h^{(2)} = \{K_i : i = 9, 10\}$.

Step 3. Repeating step 2, we obtain the non-overlapping decomposition $T_h = T_h^{(1)} \cup T_h^{(2)} \cup \dots \cup T_h^{(s)}$. The computation should follow this sequence; that is, start the computation with the elements in $T_h^{(1)}$ and end with the elements in $T_h^{(s)}$.

In the above procedure, the unknown function u_h^l on each element K is computed by following the source iteration scheme of (3.17), that is, with an initial guess $u_h^{l,0} \in P_k(K)$, $0 \leq l \leq L$, for $j = 1, 2, \dots$, we seek $u_h^{l,j} \in P_k(K)$, $0 \leq l \leq L$, such that

$$(5.1) \quad \begin{aligned} & \left(\boldsymbol{\omega}_l \cdot \nabla u_h^{l,j} + \sigma_t u_h^{l,j}, v_h^l + \delta \boldsymbol{\omega}_l \cdot \nabla v_h^{l,j} \right)_K + \left\langle [u_h^{l,j}], v_+^l |\boldsymbol{\omega}_l \cdot \mathbf{n}| \right\rangle_{\partial_-^l K} \\ & = \left(\sigma_s \sum_{i=0}^L w_i g(\cdot, \boldsymbol{\omega}_i \cdot \boldsymbol{\omega}_i) u_h^{i,j-1} + f_l, v_h^l + \delta \boldsymbol{\omega}_l \cdot \nabla v_h^l \right)_K \quad \forall v_h^l \in P_k(K) \end{aligned}$$

with

$$(5.2) \quad u_-^{l,j}|_{\partial_-^l K} = 0, \quad \partial_-^l K \subset \partial_-^l X.$$

For any $K \in T_h$ and $v_h \in P_k(K)$, it is easy to prove that there exists a positive constant C_K satisfying

$$\begin{aligned} C_K & \left(\|v_h\|_{0,K}^2 + \delta \|\boldsymbol{\omega}_l \cdot \nabla v_h\|_{0,K}^2 + \frac{1}{2} \left\langle v_-^l, v_-^l |\boldsymbol{\omega}_l \cdot \mathbf{n}| \right\rangle_{\partial_+^l K} \right) \\ & \leq (\boldsymbol{\omega}_l \cdot \nabla v_h + \sigma_t v_h, v_h + \delta \boldsymbol{\omega}_l \cdot \nabla v_h)_K + \left\langle v_+^l, v_+^l |\boldsymbol{\omega}_l \cdot \mathbf{n}| \right\rangle_{\partial_-^l K} \end{aligned}$$

when h is sufficiently small. Then the unique solvability of (5.1)–(5.2) can be obtained by the above inequality and the Lax-Milgram lemma (see e.g. [10]).

We perform the above procedure for all directions in one iteration step, and stop the iteration if some stopping condition is met, and take $\{u_h^{l,j}\}$ as $\{u_h^l\}$.

5.2. Numerical experiments. Let $X = (0, 1) \times (0, 1)$. We consider the following four examples of the radiative transfer equation (2.3)–(2.4):

Example 1. the H-G phase function with $\eta = 0.2$.

Example 2. the H-G phase function with $\eta = 0.5$.

Example 3. the H-G phase function with $\eta = 0.9$.

Example 4. the phase function

$$g(\mathbf{x}, t) = \frac{1}{2\pi} \left(1 + \frac{t}{2} \right).$$

For **Example 1** - **Example 3**, the true solution is

$$u(\mathbf{x}, \boldsymbol{\omega}) = \sin(\pi x_1) \sin(\pi x_2).$$

And for **Example 4**, the true solution is

$$u(\mathbf{x}, \boldsymbol{\omega}) = e^{-ax_1 - bx_2} (1 + c \cos \theta),$$

with $a = b = \frac{\sigma_a}{3}$ and $c = \frac{\sigma_a}{\sigma_a + 6\sigma_s}$. We set the right hand function $f(\mathbf{x}, \boldsymbol{\omega})$ to satisfy the radiative transfer equation.

Let $T_0 = T_{h_0}$ be an initial triangulation of X with a mesh size $h_0 \approx 0.1$. Then we recursively generate a sequence of nested triangulations $T_l = T_{h_l}$, $l = 1, 2, 3$, by dividing each triangle in the previous mesh T_{l-1} into four sub-triangles by connecting the midpoints of the edges; $h_l = 2^{-l}h_0$. Based on these meshes, the linear finite element spaces are constructed and used in the spatial discretization. For the angular discretization, we employ the composite trapezoidal rule (3.3) with $h_\theta = \pi/10, \pi/20, \pi/30$ and $\pi/10$ for the above four examples respectively.

We shall use the DODSD method with $\delta = h_l$ to solve these examples. To measure the difference between the true solution and its approximate solution, we define the quantity $|||u - u_h|||_h := \left(\sum_{i=1}^4 (|||u - u_h|||^{(i)})^2 \right)^{\frac{1}{2}}$ with

$$\begin{aligned} |||v|||^{(1)} &= \left(\sum_{l=0}^L w_l \sum_{K \in T_h} \|v^l\|_{0,K}^2 \right)^{\frac{1}{2}}, & |||v|||^{(2)} &= \left(\sum_{l=0}^L w_l \sum_{\partial_+^l K \subset \partial_+^l X} \langle v_-^l, v_-^l \boldsymbol{\omega}_l \cdot \mathbf{n} \rangle_{\partial_+^l K} \right)^{\frac{1}{2}}, \\ |||v|||^{(3)} &= \left(\sum_{l=0}^L w_l \sum_{K \in T_h} h_K \|\boldsymbol{\omega}_l \cdot \nabla v^l\|_{0,K}^2 \right)^{\frac{1}{2}}, & |||v|||^{(4)} &= \left(\sum_{l=0}^L w_l \sum_{K \in T_h} \langle [v^l], [v^l] \boldsymbol{\omega}_l \cdot \mathbf{n} \rangle_{\partial_-^l K} \right)^{\frac{1}{2}}. \end{aligned}$$

5.2.1. *Numerical convergence rates.* In this subsection, we take $\sigma_t = 10$, $\sigma_s = 0.1$. Errors for these four examples are reported in Table 1–Table 4 and Figure 3–Figure 6. For all these examples, we can see that $|||u - u_h|||^{(i)}$, $i = 1, 2, 3$, are approximately $O(h^2)$, and that $|||u - u_h|||^{(4)} \approx O(h^{1.5})$. Since $|||u - u_h||| \approx |||u - u_h|||_h$, we can conclude that $|||u - u_h||| = O(h^{1.5})$ for all these examples, which agrees with our theoretical error estimates.

TABLE 1. Error for Example 1

l	$ u - u_h ^{(1)}$	$ u - u_h ^{(2)}$	$ u - u_h ^{(3)}$	$ u - u_h ^{(4)}$	$ u - u_h _h$
0	5.3989e-3	6.1012e-3	7.6011e-2	3.3398e-2	8.3424e-2
1	1.3923e-3	1.6388e-3	2.6936e-2	1.2970e-2	2.9973e-2
2	3.5459e-4	4.3395e-4	9.5335e-3	4.8451e-3	1.0709e-2
3	8.9879e-5	1.1300e-4	3.3722e-3	1.7661e-3	3.8094e-3

5.2.2. *Comparison with the DODG method.* In order to show the effects of adding the artificial diffusion term, we report the error of the DODG method in norm $||| \cdot |||_h$ for the four examples in Table 5. The comparisons of the DODSD method and the DODG method are also shown in Figure 7. We observe that: 1) both the DODSD method and the DODG method have the similar convergence rates; 2) the DODSD method can lead to some improvement of the accuracy in norm $||| \cdot |||_h$ compared to the DODG method.

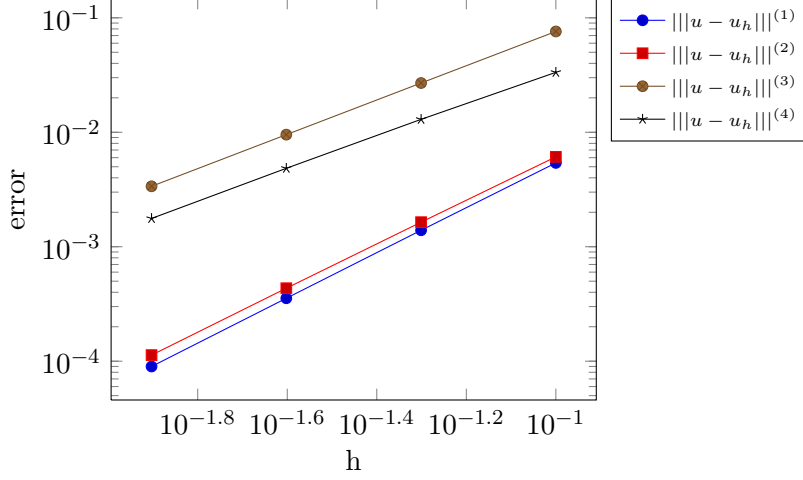
FIGURE 3. Loglog convergence plot of $|||u - u_h|||^{(i)}$ ($i = 1, 2, 3, 4$) vs. h for Example 1

TABLE 2. Error for Example 2

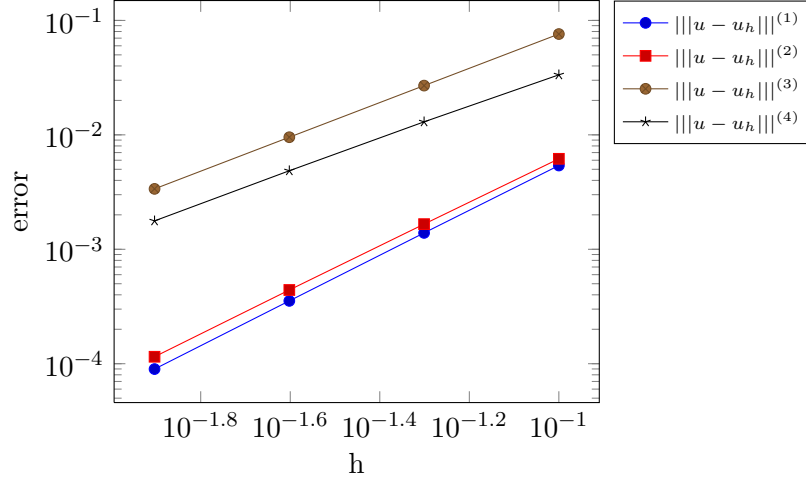
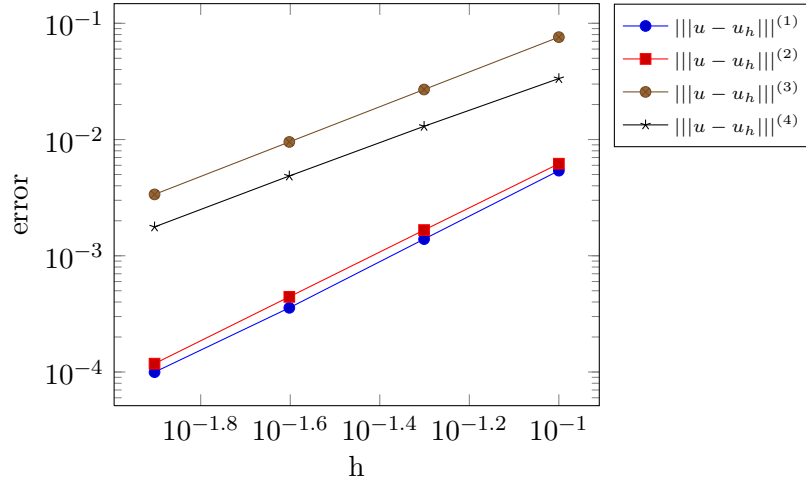
T_l	$ u - u_h ^{(1)}$	$ u - u_h ^{(2)}$	$ u - u_h ^{(3)}$	$ u - u_h ^{(4)}$	$ u - u_h _h$
0	5.3951e-3	6.1766e-3	7.6014e-2	3.3452e-2	8.3453e-2
1	1.3904e-3	1.6591e-3	2.6937e-2	1.2994e-2	2.9985e-2
2	3.5412e-4	4.4085e-4	9.5337e-3	4.8564e-3	1.0714e-2
3	8.9791e-5	1.1504e-4	3.3723e-3	1.7711e-3	3.8119e-3

TABLE 3. Error for Example 3

l	$ u - u_h ^{(1)}$	$ u - u_h ^{(2)}$	$ u - u_h ^{(3)}$	$ u - u_h ^{(4)}$	$ u - u_h _h$
0	5.3969e-3	6.1958e-3	7.6013e-2	3.3459e-2	8.3456e-2
1	1.3910e-3	1.6639e-3	2.6936e-2	1.2996e-2	2.9986e-2
2	3.5655e-4	4.4334e-4	9.5332e-3	4.8567e-3	1.0714e-2
3	9.9651e-5	1.1797e-4	3.3719e-3	1.7711e-3	3.8118e-3

6. CONCLUSION

In this paper, we present a discrete-ordinate discontinuous-streamline diffusion method for solving the radiative transfer equation. This method applies the discrete ordinate technique to deal with the integration

FIGURE 4. Loglog convergence plot of $|||u - u_h|||^{(i)}$ ($i = 1, 2, 3, 4$) vs. h for Example 2FIGURE 5. Loglog convergence plot of $|||u - u_h|||^{(i)}$ ($i = 1, 2, 3, 4$) vs. h for Example 3

term of the radiative transfer equation in the angular discretization, and employs the discontinuous-streamline diffusion method for the spatial discretization. The stability property and unique solvability of the discrete system are proved. Under suitable solution regularity assumptions, error estimates for the numerical solutions are derived in a norm including the directional gradient. Numerical results confirm the convergence behavior of the proposed method.

The main difference between the DODSD method and the DODG method is in the additional artificial diffusion term. Our numerical experiments show that such a modification can improve the accuracy of numerical solutions in term of $||| \cdot |||_h$ norm in comparison with the DODG method. As for the effect of the artificial diffusion parameter δ , we remark that it may reduce the error $|||u - u_h|||^{(3)}$ and $|||u - u_h|||^{(4)}$ while

TABLE 4. Error for Example 4

l	$ u - u_h ^{(1)}$	$ u - u_h ^{(2)}$	$ u - u_h ^{(3)}$	$ u - u_h ^{(4)}$	$ u - u_h _h$
0	3.6110e-3	2.6820e-3	3.1865e-2	1.2766e-2	3.4620e-2
1	9.1999e-4	7.8409e-4	1.1233e-2	5.1355e-3	1.2410e-2
2	2.3272e-4	2.1117e-4	3.9834e-3	1.9544e-3	4.4481e-3
3	5.8632e-5	5.5119e-5	1.4122e-3	7.1893e-4	1.5867e-3

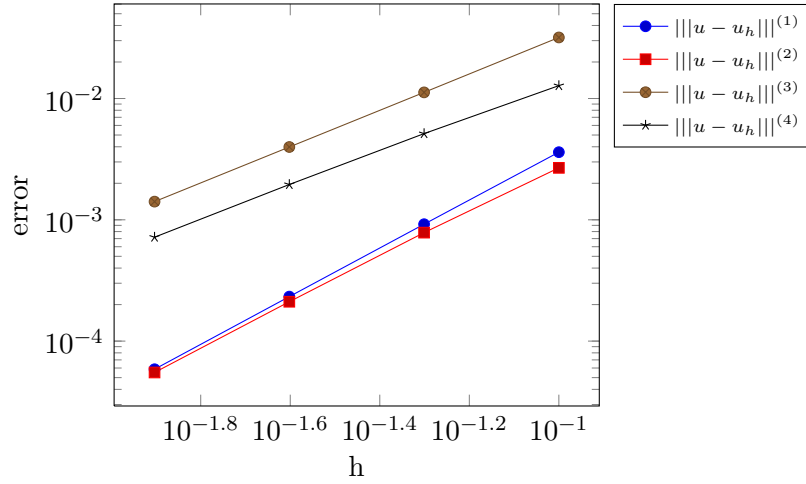
FIGURE 6. Loglog convergence plot of $|||u - u_h|||^{(i)}$ ($i = 1, 2, 3, 4$) vs. h for Example 4

TABLE 5. Results of the DODG method

l	Example 1	Example 2	Example 3	Example 4
0	9.6214e-2	9.6254e-2	9.6265e-2	3.8551e-2
1	3.5124e-2	3.5140e-2	3.5141e-2	1.4422e-2
2	1.2668e-2	1.2674e-2	1.2673e-2	5.2930e-3
3	4.5303e-3	4.5324e-3	4.5316e-3	1.9121e-3

increase the error $|||u - u_h|||^{(1)}$ and $|||u - u_h|||^{(2)}$. Since $|||u - u_h|||^{(1)}$ and $|||u - u_h|||^{(2)}$ converge faster than $|||u - u_h|||^{(3)}$ and $|||u - u_h|||^{(4)}$, the DODSD method with an appropriate δ is expected to be more accurate in $||| \cdot |||$ norm in comparison with the DODG method.

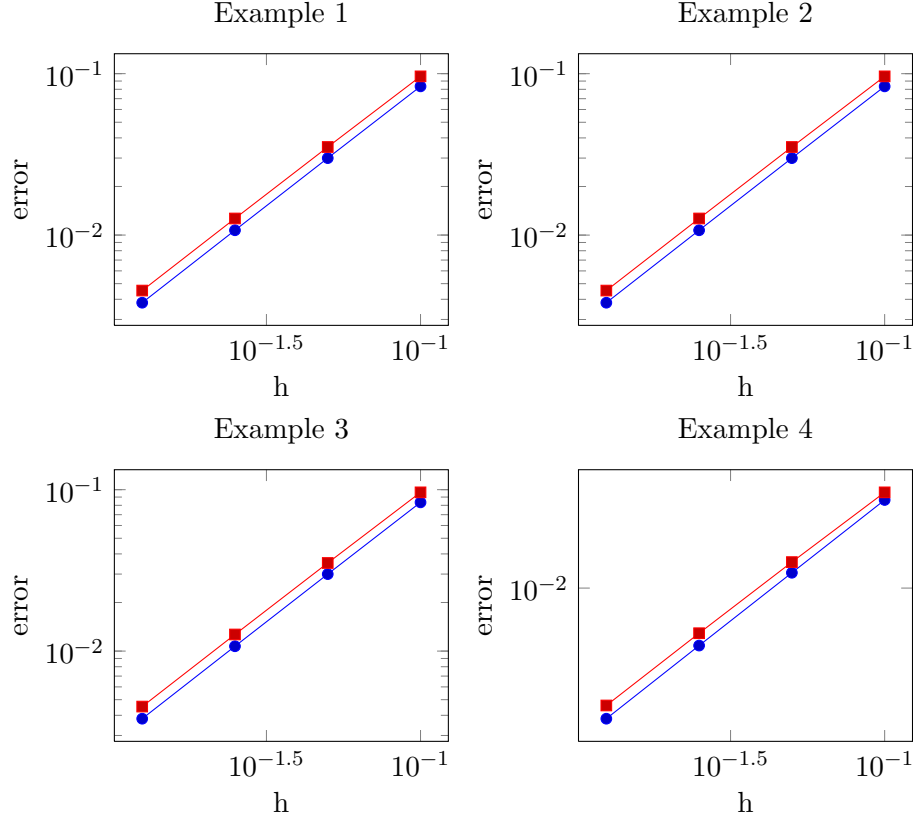


FIGURE 7. Loglog convergence plot of $|||u - u_h|||_h$ vs. h (red line: DODG method; blue line: DODSD method)

REFERENCES

- [1] V. Agoshkov. *Boundary Value Problems for Transport Equations*. Modeling and Simulation in Science, Engineering and Technology. Birkhäuser Boston, 1998.
- [2] S. R. Arridge and J. C. Schotland. Optical tomography: forward and inverse problems. *Inverse Problems*, 25(12):123010, 2009.
- [3] M. Asadzadeh and E. Kazemi. On convergence of the streamline diffusion and discontinuous galerkin methods for the multi-dimensional fermi pencil beam equation. *Int. J. Numer. Anal. Mod.*, 10(4):860–875, 2013.
- [4] M. Asadzadeh and P. Kowalczyk. Convergence analysis of the streamline diffusion and discontinuous galerkin methods for the vlasov-fokker-planck system. *Numerical Methods for Partial Differential Equations*, 21(3):472–495, 2005.
- [5] K. Atkinson. *An Introduction to Numerical Analysis*, 2nd ed. John Wiley & Sons, 1989.
- [6] G. Bal. Inverse transport theory and applications. *Inverse Problems*, 25(5):053001, 2009.
- [7] S. Brenner and R. Scott. *The Mathematical Theory of Finite Element Methods*, volume 15 of *Texts in Applied Mathematics*. Springer, 3rd edition, 2008.
- [8] B. G. Carlson. Solution of the transport equation by the S_n method. *Los Alamos National Laboratory*, 1955.
- [9] K. W. Che Sun, Huaimin Tan. The discontinuous-streamline diffusion method for first-order hyperbolic equation. *Mathematica Numerica Sinica*, 20(1):35–44, Feb. 1998.
- [10] P. Ciarlet. *The Finite Element Method for Elliptic Problems*. Society for Industrial and Applied Mathematics, 2002.

- [11] H. Egger and M. Schlottbom. A mixed variational framework for the radiative transfer equation. *Mathematical Models and Methods in Applied Sciences*, 22(03):1150014, 2012.
- [12] J. A. Fleck Jr. and J. D. Cummings Jr. An implicit Monte Carlo scheme for calculating time and frequency dependent nonlinear radiation transport. *Journal of Computational Physics*, 8(3):313–342, 1971.
- [13] H. Gao and H. Zhao. Analysis of a numerical solver for radiative transport equation. *Mathematics of Computation*, 82(281):153–172, 2013.
- [14] W. Han, J. Eichholz, X. Cheng, and G. Wang. A theoretical framework of X-ray dark-field tomography. *SIAM Journal on Applied Mathematics*, 71(5):1557–1577, 2011.
- [15] W. Han, J. Eichholz, and Q. Sheng. Theory of differential approximations of radiative transfer equation. In *Advances in Applied Mathematics and Approximation Theory*, pages 121–148. Springer, 2013.
- [16] W. Han, J. Huang, and J. Eichholz. Discrete-ordinate discontinuous Galerkin methods for solving the radiative transfer equation. *SIAM Journal on Scientific Computing*, 32(2):477–497, 2010.
- [17] W. Han, Y. Li, Q. Sheng, and J. Tang. A numerical method for generalized Fokker-Planck equations. *Recent Advances in Scientific Computing and Applications*, 586:171, 2013.
- [18] K. Hesse and I. H. Sloan. Cubature over the sphere S^2 in Sobolev spaces of arbitrary order. *J. Approx. Theory*, 141:118–133, 2006.
- [19] J. R. Howell. The Monte Carlo method in radiative heat transfer. *Journal of Heat Transfer*, 120(3):547–560, 1998.
- [20] T. J. Hughes, M. Mallet, and M. Akira. A new finite element formulation for computational fluid dynamics: II. beyond {SUPG}. *Computer Methods in Applied Mechanics and Engineering*, 54(3):341–355, 1986.
- [21] C. Johnson and U. Nävert. An analysis of some finite element methods for advection-diffusion problems. In O. Axelsson, L. Frank, and A. V. D. Sluis, editors, *Analytical and Numerical Approaches to Asymptotic Problems in Analysis Proceedings of the Conference on Analytical and Numerical Approaches to Asymptotic Problems*, volume 47 of *North-Holland Mathematics Studies*, pages 99–116. North-Holland, 1981.
- [22] R. Koch, W. Krebs, S. Wittig, and R. Viskanta. The discrete ordinate quadrature schemes for multidimensional radiative transfer. *Journal of Quantitative Spectroscopy and Radiative Transfer*, 53, 1995.
- [23] E. W. Larsen and J. E. Morel. Advances in discrete-ordinates methodology. In *Nuclear Computational Science*, pages 1–84. Springer Netherlands, 2010.
- [24] I. Lux and K. L. *Monte Carlo Particle Transport Methods: Neutron and Photon Calculations*. CRC Press, 1991.
- [25] R. G. McClarren and C. D. Hauck. Simulating radiative transfer with filtered spherical harmonics. *Physics Letters A*, 374(22):2290–2296, 2010.
- [26] K. Ren. Recent developments in numerical techniques for transport-based medical imaging methods. *Communications in Computational Physics*, 8:1–50, 2010.
- [27] J. Spanier and E. Gelbard. *Monte Carlo Principles and Neutron Transport Problems*. Dover, New York, 2008.
- [28] J. Tang, W. Han, and B. Han. A theoretical study for RTE-based parameter identification problems. *Inverse Problems*, 29(9):095002, 2013.